Decoding Urban Heat: A Decadal Analysis (1991-2021) of Land Surface Temperature and Thermal Comfort Dynamics in Coastal Taluka of Bardez, Goa, India

Gaonkar Venkatesh Prabhu[1,2], Nadaf F.M.[3]* and Kapale Vikas[4]

1. Department of Geoinformatics, Government College of Commerce & Economics, Borda Margao, Goa (Autonomous), INDIA
2. Goa University, Cluster Research Centre of Geography, Government College of Arts, Science & Commerce, Khandola, Marcela, Goa, INDIA
3. Government College of Commerce & Economics, Borda Margao, Goa (Autonomous), INDIA
4. Indian Institute of Technology, Kanpur, INDIA

*fmnadaf@gmail.com

Abstract

The urban heat island phenomenon refers to the alteration of the climate in urban areas resulting from the disruptions caused by urban development. This issue is of immense concern for the vast number of individuals living in cities. The rural regions across the world are diminishing at a rapid rate, leading to significant transformations in land use and land cover. The dynamics of urban thermal comfort is closely linked to these changes. The assessment of urban thermal comfort levels can be accomplished through the utilization of the urban thermal field variance index (UTFVI) which is derived from LST data. The study reveals that Bardez taluka, located in Goa, India, has witnessed substantial alterations in land use and land cover over the past three decades, primarily due to economic advancement and population growth. From 1991 to 2021, the Urban thermal field variance index (UTFVI) in the Bardez taluka has shown a clear upward trend, indicating increased temperature fluctuations in urban areas. This rise has negative effects on residents' comfort, as the size of land offering "excellent" comfort has decreased from 37.30 sq. km (14.76%) in 1991 to 27.05 sq. km (10.71%) in 2021 showing a decrease of 4.05 %.

Conversely, areas with the "worst" comfort level have increased from 13.98 sq. km (5.54%) to 38.17 sq. km (15.11%) showing a 9.57% increase during the same period. These changes are influenced by factors like urbanization, impenetrable surfaces like asphalt and concrete, towering structures and crowded infrastructure, minimal green areas, altered microclimate, human actions such as industrial processes, transportation and energy consumption, which can create urban heat islands and raise overall temperatures in cities. These findings carry significant implications for urban planning, policy-making and sustainable development. In addition, the study provides important insights into the consequences of anthropogenic actions and alterations in land use on urban heat and thermal comfort.

**** Author for Correspondence***

Keywords: Urban Heat, Land Surface Temperature, Land Use and Land Cover, Thermal Comfort, Remote Sensing, GIS.

Introduction

Earth is presently confronting a variety of challenges and one noteworthy concern is the issue of urban heat. Urban regions are encountering an upswing in temperatures in comparison to their rural counterparts[32]. This increase in temperature can be ascribed to a combination of natural elements and human activities, encompassing climate change, industrialization, urbanization and modifications in land use and land cover[18]. These elements collectively contribute to the occurrence of urban heat, presenting difficulties that call for meticulous consideration and strategic interventions[66]. Decoding urban heat involves understanding the relationship between different factors such as land surface temperature (LST), air temperature and urban structure[2].

Land is a crucial natural resource that is necessary for human survival and serves as the basis for all functions of terrestrial ecosystems[1,14,21] which act as an asset due to the interaction between factors such as topography, environment, climate and soil, as well as human aspects such as demographics, technical capabilities and cultural and traditional activities[42]. Over the past century, there have been significant changes in land use and land cover on a regional and temporal scale[1]. These changes have primarily occurred as a result of economic progress and population growth. Unfortunately, due to unsustainable human actions, the physical environment is experiencing alarming and extensive changes[43,46]. More than 50% of the global population now resides in urban areas, marking the era of the "urban century"[12,17].

The alteration of land use and land cover is a major environmental change happening worldwide[4]. It is crucial to comprehend how these changes interact with climate, ecological processes, biodiversity and human activities[4,27,57]. Since different land uses and land covers have distinct characteristics in terms of energy radiation and absorption, the conversion of land use and land cover changes is the primary cause for modifying land surface temperature (LST)[5,9]. The temperature of bare ground is often higher than that of other settings such as forests or agricultural fields[15,47,75].

The impact of tourism on land cover and the environment is especially severe in coastal areas, resulting in a decline in water bodies and vegetation and an increase in built-up areas[35,44,49,76]. The conditions in tourism areas are deteriorating due to improper land use and land cover practices including deforestation, tourism-related activities and urban development at various scales[4,11].

Urbanization modifies the local urban climate by increasing LST [56,61]. Research has shown a strong correlation between LST and changes in land use and land cover classes[55,70,72]. It can be inferred that LST and land use and land cover changes are closely related since the conversion of land use and land cover leads to urban heat island effects and subsequently affects the local climate[32,71,73]. The urban thermal field variance index (UTFVI) is calculated using LST [40] which is commonly used to study urban thermal comfort levels. The concentration of UTFVI is higher in places that are significantly warmer than the surrounding rural regions[44,69]. To measure the level of urban thermal comfort, research has been conducted using the urban thermal field variance index[13,23, 26,28,34,39,41,44,60].

Bardez is the most prominent administrative division of North Goa, India, known for tourism activities and rapid urban expansion. The main goal of this study is to understand changes in land use, to calculate the UTFVI using geospatial and geostatistical approaches like linear regression and to identify optimal urban comfort zones in the research area. Further, this research attempts to examine the land use land cover pattern in conjunction with LST. UTFVI technique can help to control future changes caused by land use, land cover and land surface temperatures.

Material and Methods

Study Area: The primary focus of ongoing research is Bardez taluka, a well-known administrative subdivision located in the northern part of Goa, which is not only acknowledged for its geographical importance but also renowned as a prominent global tourist destination. Positioned strategically, this taluka is bounded by the Chapora River in the north, the Mandovi River in the south, the Mapusa River in the east and the majestic Arabian Sea in the west (Fig. 1 and fig. 2). Bardez taluka extends across the latitudinal coordinates of 15°37'17.15"N to 15°35'23.66"N and the longitudinal coordinates of 73°48'0.73"E to 73°51'50.35"E, encompassing an exceptionally diverse and environmentally significant area for thorough examination and evaluation.

Database and Methodology: Fig. 3 illustrates the methodological flow chart outlining the different steps in processing and analysis. Processing involves image processing such as radiometric and geometric corrections, while analysis includes creating land use land cover maps, accuracy assessments, retrieval of LST, estimation of surface urban heat island, urban thermal field variance index, urban thermal comfort level and stack profile.

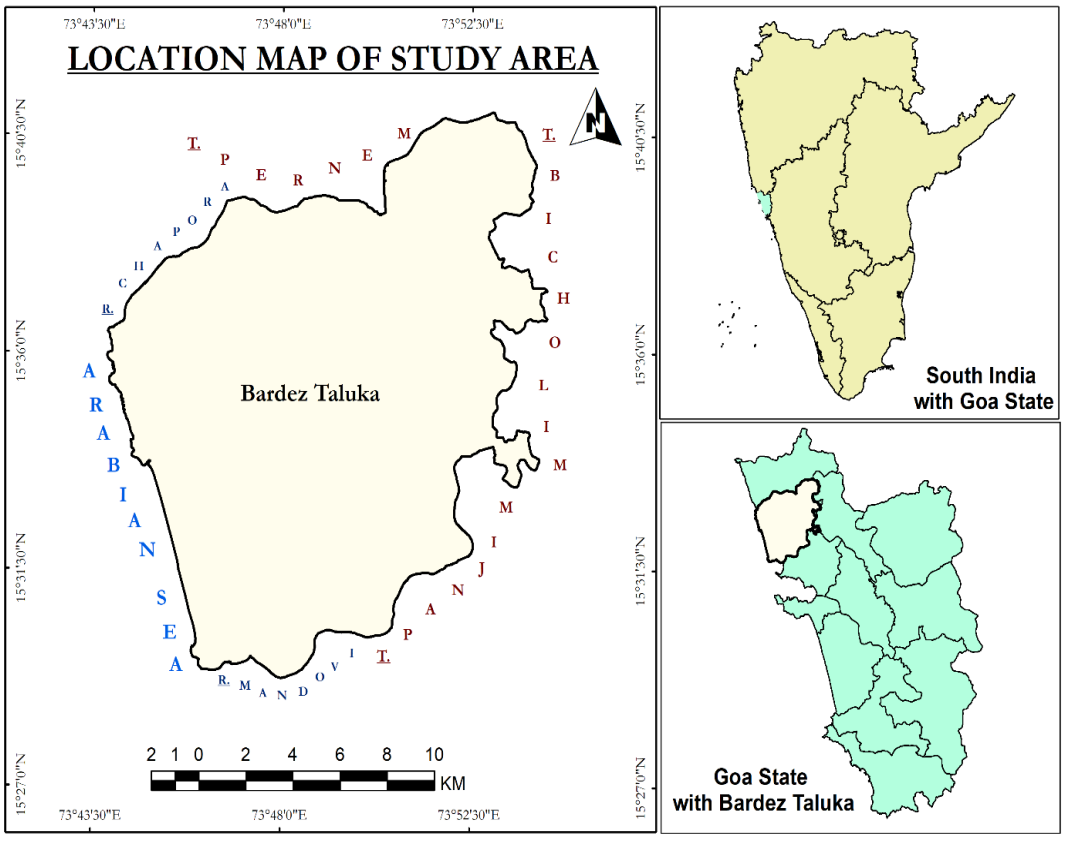

Figure 1: Location Map of Bardez Taluka

The study is based on both primary and secondary sources. The primary data was obtained from field observations as well as ground truthing. The secondary data includes the LANDSAT satellite images from 1991 and 2000 obtained from earthexplorer.usgs.gov. There was no cloud cover in both images. The satellite images were captured in February, during the spring season when tree canopies are in full bloom (Table 1).

Image processing and hybrid classification: In image processing, for classification and LST, ERDAS Imagine 15 software was used to apply atmospheric and radiometric corrections to improve accuracy and to eliminate errors in preparation for subsequent calibrations. The corrected data was used for classification purposes. To perform hybrid classification, the study area was determined by overlaying the study region's shape file on satellite images from 1991 and 2021. Anderson level II classification scheme[7,30,52,59] was opted for the land use land cover classification. The study area was classified into 19 major classes. The clipped area was later digitized as tidal river, fresh water bodies, salt pans, forested wetlands, non-forested wetlands, agricultural land, coconut plantation, cashew plantation, barren land, bare exposed rocks, sand dunes and sandy area, residential, commercial and services, mining, transportation and utilities, DM and FDM forest land, open scrub and fairly open scrub, industrial and fallow land[8,68].

The data derived from the LULC classification aids in comprehending the positive and negative developments in Bardez taluka. ArcMap version 10.8 was utilized for classifying the data, facilitating comparative analysis of spatio-temporal changes from 1991 to 2021.

Later, the technique of accuracy assessments was performed for a better understanding of the accuracy of LULC maps derived from on-screen digitization (hybrid classification) [29,54]. The Kappa coefficient is a tool that helps to measure the agreement between collected data and reference data [16,22,53]. In total, 152 random points were chosen in the study area to calculate accuracy for the years 1991 and 2021. The formulas for accuracy assessment in 1991 and 2021 were derived accordingly[6,37].

Users Accuracy

$$= \frac{No.\ of\ Correctly\ Clasified\ Pixels \in Category}{The\ Row\ Total} * 100 \quad (1)$$

Produced Accuracy

$$= \frac{No.\ of\ Correctly\ Clasified\ Pixels \in Category}{The\ Column\ Total} * 100 \quad (2)$$

Overall Accuracy

$$= \frac{Total\ no.\ of\ correctly\ classified\ pixels\ (diagonals)}{Total\ no.\ of\ reference\ pixels} * 100 \quad (3)$$

Kappa Coefficient

$$= \frac{(TS*TCS)-\sum(Column\ Total * Row\ Total)}{TS^2-\sum(Column\ Total * Row\ Total)} * 100 \quad (4)$$

where TS = corrected sample and TCS = total corrected sample.

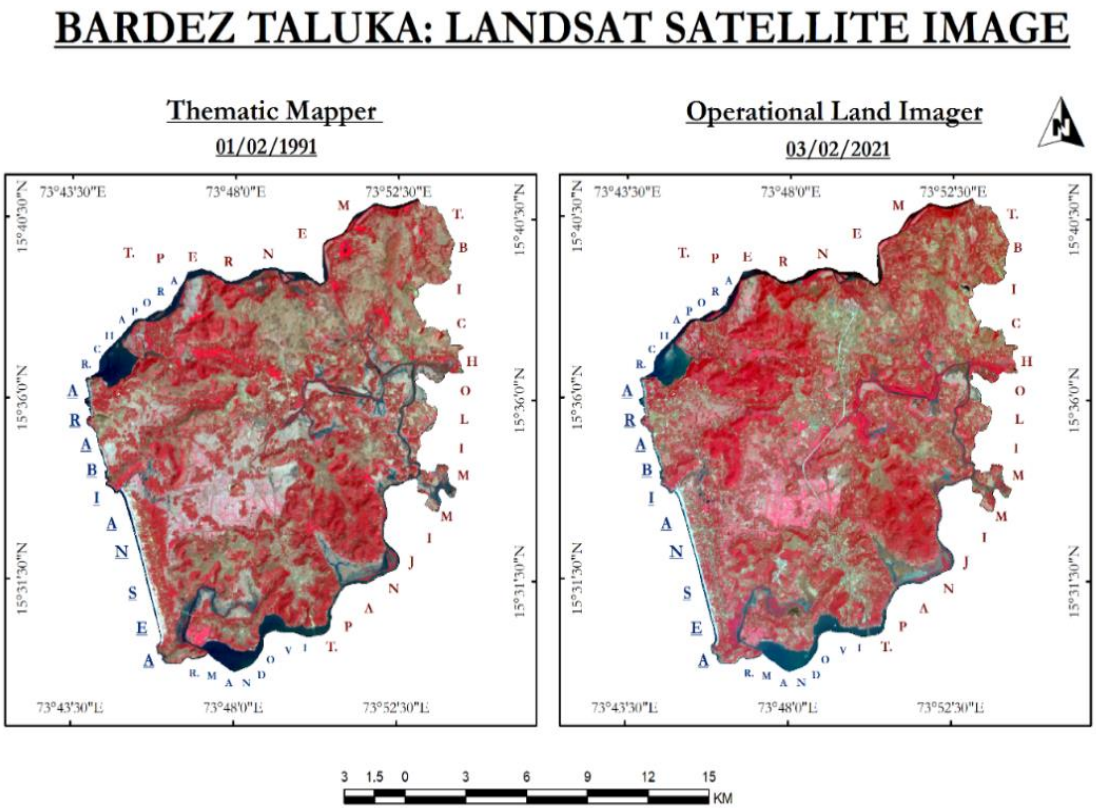

Figure 2: Database Maps of Study Location.

Table 1
Database of study location

Satellite	Path	Row	Date	Cloud Cover
LANDSAT (TM)	147	049	01/02/1991	0
LANDSAT (OLI)	147	049	03/02/2021	0

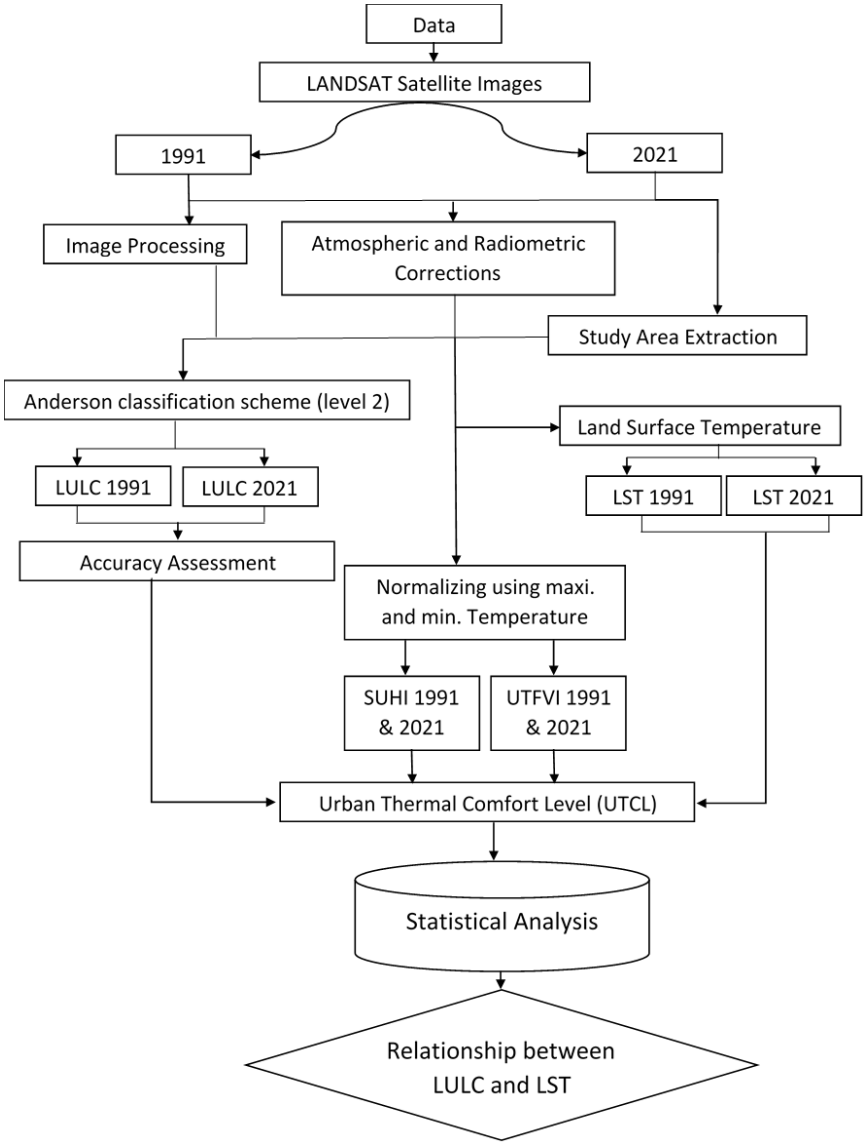

Figure 3: Methodological Framework

The evaluation of the LULC Classification for 1991 and 2021 involved comparing it with Landsat - 5 (TM) and Landsat -8 (OLI) natural color data, merging bands from these satellites and presenting them using RGB color combinations 3, 2, 1 for Landsat - 5 and 4, 3, 2 for Landsat - 8[19,65,74].

Retrieval of LST: LANDSAT TM and OLI satellite images were used to obtain land surface temperature. The thematic mapper's thermal band was band 6 (10.40 µm- 12.50µm) with a spatial resolution of 120 meters [44], while the OLI thermal bands were band 10 (10.60 µm- 11.19) and band 11 (11.50 µm- 12.51µm) with a spatial resolution of 100 meters[2,48,58]. The data from both years were later re-sampled to 30-meter resolution using the pan-sharpen tool in ArcMap 10.8.

Using eqs. (5) and (6) for Landsat 5 and Landsat 8, respectively, digital numbers (DN) were converted to radiance.

$$L_\lambda = \left(\frac{L_{max\lambda} - L_{min\lambda}}{QCal_{max} - QCal_{min}}\right) * (QCal - QCal_{min}) + L_{min\lambda}a \quad (5)$$

Equation (1) was used for Landsat TM where [44], L_λ = Spectral radiance, $L_{max\lambda}$ = Maximum spectral radiance of band 6, $L_{min\lambda}$ = Maximum spectral radiance of band 6, $QCal_{max}$= maximum digital number (DN) of the band 6,

$QCal_{min}$= minimum digital number (DN) of the band 6, $QCal$ = bands' digital value (DN), which ranges from 0 to 255 [31].

$$L_\lambda = M_L \times Q_{Cal} \times A_L \quad (6)$$

Equation (2) was obtained for Landsat OLI from[33] where L_λ = Spectral radiance, M_L= scaling factor for multiplicative radiance, Q_{Cal} =bands (DN) value, A_L= band radiance additive scaling factor for band 10 and band 11 obtained from metadata of the satellite imagery[10,24,63].

Secondly, to calculate Brightness temperature in ^{0}C spectral radiance was further calculated. Eq. (7) was used for calculation purposes:

$$BT = \frac{K_2}{log\left(\frac{K_1}{\lambda_1}+1\right)} - 273.15 \quad (7)$$

where BT = Top of atmospheric brightness temperature (°C), λ_1 = Top of atmosphere (TOA) spectral radiance, $K_2$and K_1 are the calibration constants of the thermal band of Landsat 5 and Landsat 8.

Thirdly, the normalized difference vegetation index (NDVI) was calculated by considering the output of brightness temperature. Normalized difference vegetation index is the standardized vegetation index which is calculated using two bands of Landsat 8 and Landsat 5 namely, for Landsat 8 OLI (band 5) infrared band and (band 4) red band and Landsat 5 TM (band 4) infrared band and (band 3) red band respectively[25,64,67].

$$NDVI = \frac{NIR-R}{NIR+R} \quad (8)$$

where NIR = Near Infrared Band and R = Red band of Landsat satellite imageries.

Fourthly, to calculate the proportion of vegetation, it is important to consider the values of eq. (8). Eq. (9) is used for the calculation of Pv[3,45].

$$Pv = \left[\frac{NDVI-NDVI_{min}}{NDVI_{max}-NDVI_{min}}\right]^2 \quad (9)$$

where Pv = proportion of vegetation, $NDVI$ = Normalized Difference Vegetation Index, $NDVI_{min}$= Minimum DN value of NDVI output and $NDVI_{max}$= Maximum DN value of NDVI output.

The output of Pv helped to calculate land surface emissivity. The emissivity is obtained from eq. (10)[44]:

$$\varepsilon = 0.004 \times Pv + 0.986 \quad (10)$$

where ε = emissivity, Pv= calculated proportion of vegetation using eq. (10) and value 0.986 is the corresponding value of the equation.

Lastly, to retrieve land surface temperature, inputs were taken from eq.

$$LST = \frac{T}{1+\left(\frac{\lambda T}{c2}\right)*ln(\varepsilon)} \quad (11)$$

where BT = Top of atmosphere brightness temperature (°C), λ = wavelength of emitted radiance, ε = land surface emissivity and $c2$=, Constant value obtained by the formula h * c / s [20,36,51].

Estimation of SUHI and UTFVI: Based on the literature, determining SUHI involves measuring temperature in urban and rural areas [31] simultaneously to find the temperature difference, which typically shows urban areas being warmer. SUHI is computed with equation (12) and UTFVI is used to quantify SUHI vulnerability in the study area with equation (13) [13,34,38,50].

$$SUHI = \frac{T_s-T_m}{STD} \quad (12)$$

where T_s = land surface temperature, T_m = mean of the land surface temperature of the study area and STD = standard deviation.

$$UTFVI = \frac{T_s-T_m}{T_m} \quad (13)$$

where T_s = land surface temperature and T_m = mean of the land surface temperature of the study area.

Results and Discussion

To understand the changes in Land Use and Land Cover (LULC) from 1991 to 2021, figures 4 and 5, along with table 2 were created for detailed analysis of the study area. In 1991, the landscape was mainly characterized by coconut and cashew plantations, barren land, residential areas as well as DM and FDM forest cover (Dense Moist and Fragmented Dense Moist).

More precisely, coconut plantations covered an area of 15.47 sq. km (6.15%), while barren land spanned over 58.13 sq. km of areas (23%), residential areas accounted for 27.94 sq. km (11.15%) and DM and FDM forests made up 32.14 sq. km (12.72%).

In 2021, there were significant changes in all 19 land use classes, with a noticeable 2.74% decrease in coconut plantation area (Table 2). In 2021, some of the coconut plantation land was converted into residential (1.37 sq. km), commercial and services (5.54 sq. km) and transportation and utilities (0.05 sq. km) purposes, making a total of 6.96 sq. km out of the original 13.89 sq. km (Fig. 6). In the same way, land that was once used for growing cashew trees, was transformed into residential (0.83 sq. km) and commercial and service areas (0.85 sq. km), amounting to a total of 1.73 sq. km (Fig. 6). The growing tourism industry was mainly responsible for these changes.

From 1991 to 2021, the area of barren land decreased significantly by 5.99%, dropping from 58.13 sq. km to 42.99 sq. km. During this shift, barren land was transformed into residential purpose (5.06 sq. km), commercial and services (7.00 sq. km) and industry (1.87 sq. km), as shown in figure 6. Additionally, there was a notable increase in the area of freshwater bodies, rising from 0.14 sq. km in 1991 to 0.083 sq. km in 2021, due to the development of a canal for household and agricultural use (Table 2).

Approximately 0.42 sq. km of residential land was changed to commercial and service use while agricultural land, coconut and cashew plantations, barren land, DM and FDM forest cover and open scrub together added 10.53 sq. km to the growth of residential areas (Figures 6 and 7). As a result, the area of residential land grew from 27.94 sq. km in 1991 to 38.07 sq. km in 2021. Notably, there was a significant increase in the area of commercial and service land which grew from 3.72 sq. km to 24.32 sq. km, representing 80% increase. The increase was primarily fueled by the tourism sector and urban sprawl, particularly in the outskirts extending towards Porvorim (Figure 5).

Observations revealed a decline in the area of DM and FDM forest cover and open scrub from 27.02 sq. km and 14.83 sq. km in 1991 to 2021 respectively, with no change in their total combined area. Significantly, land that was once labelled as DM and FDM forest cover was converted for residential and commercial purposes (Figures 6 and 7). To sum up, the rise in tourism and associated activities has led to modifications in two LULC categories (Residential and Commercial and Services) from 1991 to 2021 as shown in figures 4, 5 and 6 and table 2.

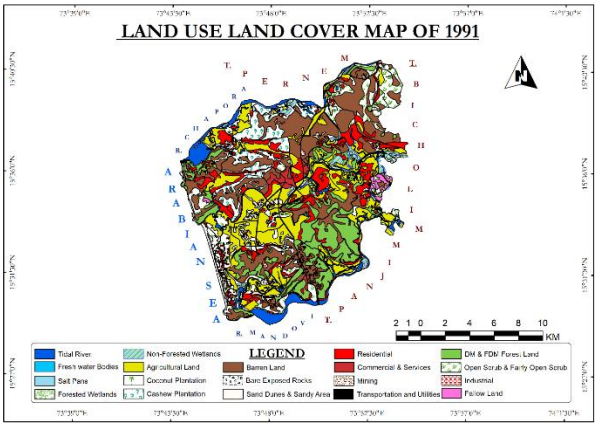

Figure 4: LULC 1991

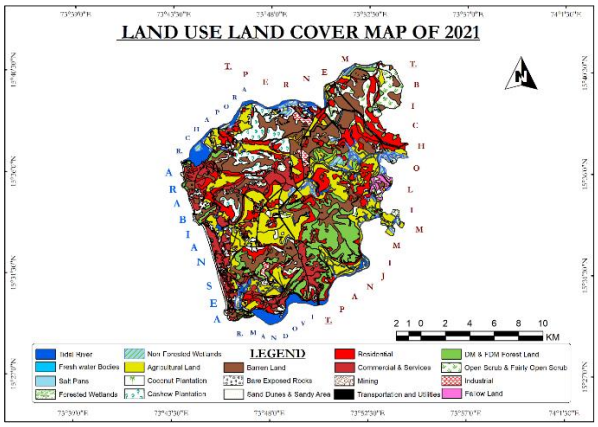

Figure 5: LULC 2021

Table 2
Percentage change in area from 1991 to 2021

Classes	**1991 Sq. Km.**	**1991 %**	**2021 Sq. Km.**	**2021 %**	**% (Increased/Decreased)**
Tidal River	16.42	6.59	15.87	6.28	-0.31
Fresh water bodies	0.14	0.05	0.83	0.33	0.28
Salt Pans	0.11	0.04	0.17	0.07	0.03
Forested Wetland	5.15	2.09	6.09	2.41	0.32
Non-forested wetland	4.57	1.8	4.47	1.77	-0.03
Agricultural Land	47.94	18.98	45.63	18.06	-0.92
Coconut Plantation	13.89	5.49	6.95	2.75	-2.74
Cashew Plantation	15.47	6.15	13.69	5.42	-0.73
Fallow Land	1.73	0.68	1.49	0.59	-0.09
Barren Land	58.13	23	42.99	17.01	-5.99
Rocky Areas	0.53	0.4	0.66	0.26	-0.14
Sand dunes and Sandy Area	2.22	0.87	1.62	0.64	-0.23
Residential	27.94	11.15	38.07	15.07	3.92
Commercial and Services	3.72	1.47	24.32	9.63	8.16
Industrial	0.31	0.12	2.20	0.87	0.75
Transportation and Services	4.08	1.17	4.79	1.90	0.73
DM and FDM Forest Land	32.14	12.72	27.06	10.71	-2.01
Open scrub and Fairly Open scrub	17.95	7.14	15.42	6.10	-1.04
Mining	0.21	0.09	0.34	0.13	0.04
Total	**252.66**	**100**	**252.66**	**100**	

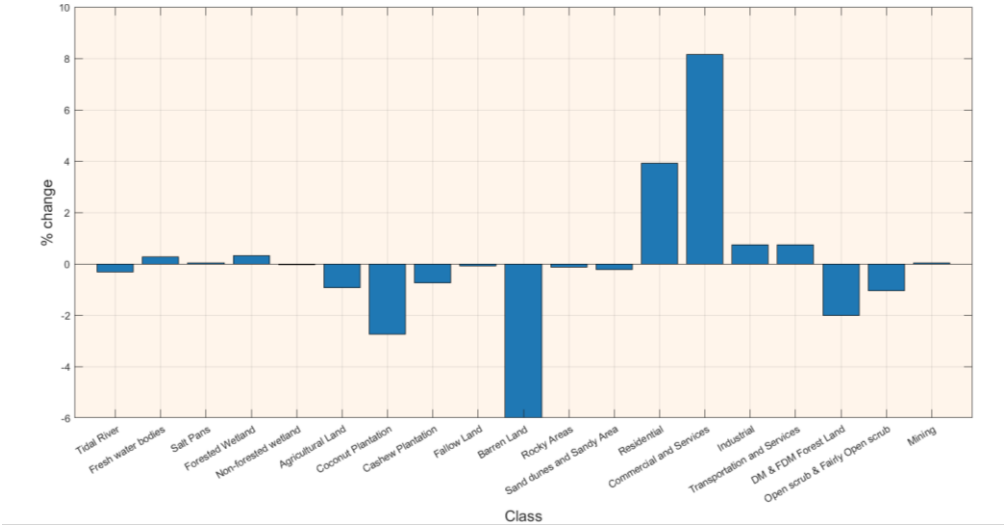

Figure 6: Percentage change in area from 1991 to 2021.

2021 \ 1991	Tidal River	Fresh water bodies	Salt Pans	Forested Wetland	Non-forested wetland	Agricultural Land	Coconut Plantation	Cashew Plantation	Fallow Land	Barren Land	Rocky Areas	Sand dunes & Sandy Area	Residential	Commercial & Services	Industrial	Transportation & Services	DM & FDM Forest Land	Open scrub & Fairly Open scrub	Mining	Total
Tidal River	15.32			0.10	0.21	0.14	0.02					0.05						0.03		15.87
Fresh water bodies		0.14				0.01		0.05		0.53								0.05	0.05	0.83
Salt Pans			0.11			0.05														0.17
Forested Wetland	0.54			4.87	0.49	0.12											0.07			6.09
Non-forested wetland	0.45			0.16	3.80	0.01											0.02			4.47
Agricultural Land	0.02				0.05	45.29			0.24											45.63
Coconut Plantation						0.02	6.90					0.03								6.95
Cashew Plantation								13.69												13.69
Fallow Land									1.49											1.49
Barren Land										42.57							0.02	0.37	0.03	42.99
Rocky Areas							0.02			0.03	0.53						0.06	0.03		0.66
Sand dunes and Sandy Area	0.05											1.55								1.62
Residential						0.60	1.37	0.83		5.06		0.01	27.52				1.66	1.01		38.07
Commercial and Services						1.51	5.54	0.85		7.00		0.58	0.42	3.72			3.25	1.53		24.32
Industrial										1.87					0.31		0.02			2.20
Transportation and Services	0.04			0.02	0.02	0.19	0.05	0.05		0.28						4.07	0.01	0.07		4.79
DM & FDM Jungle										0.04							27.02			27.06
Open scrub & Fairly Open scrub										0.59								14.83		15.42
Mining										0.17								0.03	0.14	0.34
Total	16.42	0.14	0.11	5.15	4.57	47.94	13.89	15.47	1.73	58.13	0.53	2.22	27.94	3.72	0.31	4.08	32.14	17.95	0.21	252.66
					Stable area				Negative Change				Positive Change							

Figure 7: Transition Matrix 1991-2021

Accuracy Assessment: A confusion matrix was created using different equations to compare land use land cover classes with ground truth data and matrix 1 and matrix 2. The results are shown in matrix 1 and matrix 2. Ground-controlled points with reference maps for 1991 and 2021 are displayed in fig. 8 and fig. 9. In year 1991, classes such as tidal river, fresh water bodies, salt pans, coconut plantation, barren land, sand dunes and sandy area, residential, commercial and services, mining, DM and FDM forest land, open scrub and fairly open scrub, industrial and fallow land shared 100 % user's accuracy, while it was noticed that classes namely agricultural land (91.66%), cashew plantation and bare exposed rocks (85.71%) and non-forested wetland shared the lowest users accuracy of (75%), while in year 2021 classes such as tidal river, fresh water bodies, salt pans, forested wetland, coconut plantation, cashew plantation, fallow land, barren land, base exposed rocks, industrial,, transportation and mining gave 100% users accuracy. Remaining classes such as residential, DM and FDM forest land and open scrub and fairly open scrub (92.3%), sand dunes and sandy area (88%), agricultural land (81.61%) and among all the classes, non-forested class gave less users accuracy of 75% (table 3). If we closely look at the producer's accuracy (table 3) except classes non-forested wetland (77%,85%), forested wetland (100%, 83%), agricultural land (84.61%, 100%), sand dunes and sandy area (88.88%, 100%), residential (92.3%, 92%), commercial and services (77.77%, 70%), DM and FDM forest land (92.3%, 100%) and open scrub and fairly open scrub (92.3%, 100%) in the year 1991 and 2021 respectively, had low producers accuracy while remaining classes gave 100% producers accuracy, mainly due to the selected sites distant from the scientific unit borders, which minimize the likelihood of crossover with other scientific units and accounted for the high percentage.

Thus, in the end, it can be interpreted that overall directed classification accuracy was 93.42% and 94.73% for the years 1991 and 2021 respectively. (*T)* Kappa coefficient for the year 1991 was 92.97% and 94.38% for the year 2021.

Matrix 1
Relationship between LULC classes and Ground Truth (1991)

Classes	1	2	3	4	5	6	7	8	9	10	11	12	13	14	15	16	17	18	19	Total (User)
1	10																			**10**
2		3																		**3**
3			3																	**3**
4				8																**10**
5					6															**8**
6						11												1		**12**
7							8													**8**
8								6									1			**7**
9									4											**4**
10										13										**13**
11											6									**7**
12												8								**8**
13													12							**12**
14														7						**7**
15															3					**3**
16													1	2		8				**11**
17																	12			**12**
18																		12		**12**
19																			2	**2**
Total (Producer)	**10**	**3**	**3**	**8**	**8**	**13**	**8**	**6**	**4**	**13**	**6**	**9**	**13**	**9**	**3**	**8**	**13**	**13**	**2**	**152**

Tidal river (1), fresh water bodies (2), salt pans (3), forested wetlands (4), non-forested wetlands (5), agricultural land (6), coconut plantation (7), cashew plantation (8), fallow land (9), barren land (10), bare exposed rocks (11), sand dunes and sandy area (12), residential (13), commercial and services (14), industrial (15), transportation and utilities (16), DM and FDM forest land (17), open scrub and fairly open scrub (18) and mining (19).

Matrix 2
Relationship between LULC classes and Ground Truth (2021)

Classes	1	2	3	4	5	6	7	8	9	10	11	12	13	14	15	16	17	18	19	Total (User)
1	9				1															**10**
2		3																		**3**
3			3																	**3**
4				10																**10**
5				2	6															**8**
6						12														**12**
7							8													**8**
8								7												**7**
9									4											**4**
10										12				1						**13**
11											7									**7**
12											1	7								**8**
13													12							**12**
14														7						**7**
15															3					**3**
16													1	2		8				**11**
17																	12			**12**
18																		12		**12**
19																			2	**2**
Total (Producer)	**9**	**3**	**3**	**12**	**7**	**12**	**8**	**7**	**4**	**12**	**8**	**7**	**13**	**10**	**3**	**8**	**12**	**12**	**2**	**152**

Tidal river (1), fresh water bodies (2), salt pans (3), forested wetlands (4), non-forested wetlands (5), agricultural land (6), coconut plantation (7), cashew plantation (8), fallow land (9), barren land (10), bare exposed rocks(11), sand dunes and sandy area (12), residential (13), commercial and services (14), industrial (15), transportation and utilities (16), DM and FDM forest land (17), open scrub and fairly open scrub (18) and mining (19).

Table 3
Accuracy Assessment for the years 1991 to 2021

	Classes	% of Accuracy (1991)	% of Accuracy (2021)
User Accuracy	Tidal River	100	100
	Fresh water bodies	100	100
	Salt Pans	100	100
	Forested Wetland	80	100
	Non-forested wetland	75	75
	Agricultural Land	91.66	84.61
	Coconut Plantation	100	100
	Cashew Plantation	85.71	100
	Fallow Land	100	100
	Barren Land	100	100
	Bare exposed rocks	85.71	100
	Sand dunes and Sandy Area	100	88.88
	Residential	100	92.3
	Commercial and Services	100	77.77
	Industrial	100	100
	Transportation and Utilities	72.72	100
	DM and FDM forest land	100	92.3
	Open scrub and Fairly Open scrub	100	92.3
	Mining	100	100
Producer Accuracy	**Classes**	**% of Accuracy (1991)**	**% of Accuracy (2021)**
	Tidal River	100	100
	Fresh water bodies	100	100
	Salt Pans	100	100
	Forested Wetland	100	83
	Non-forested wetland	75	85
	Agricultural Land	84.61	100
	Coconut Plantation	100	100
	Cashew Plantation	100	100
	Fallow Land	100	100
	Barren Land	100	100
	Bare exposed rocks	100	87
	Sand dunes and Sandy Area	88.88	100
	Residential	92.3	92
	Commercial and Services	77.77	70
	Industrial	100	100
	Transportation and Utilities	100	100
	DM and FDM forest land	92.3	100
	Open scrub and Fairly Open scrub	92.3	100
	Mining	100	100
Overall Accuracy		**93.42 %**	**94.73 %**
(T) Kappa Coefficient		**92.97 %**	**94.38 %**

Retrieval of LST

The increase in land surface temperature (LST) over the study period was attributed to a decrease in vegetation cover and an increase in impervious surfaces, mainly in built-up areas such as residential and commercial services (Table 2) as shown in fig. 10. To better understand LST, the area was divided into five major classes: class 1: 16-20, class 2: 20-24, class 3: 24-28, class 4: 28-32 and class 5: 32-36. In 1991, the lowest temperature was in class 16-20 °C, while in 2021, it was in class 20-24 °C. The minimum temperature of the study area has also changed over the last three decades (Fig. 10). The highest LST temperature varied between 1991 and 2021, with the highest temperature in 1991 being in class 28-32, while in 2021, heating in the study area had increased, particularly in built-up areas and barren land (Fig. 13 and 14).

Estimation of SUHI and UTFVI: The surface urban heat index (SUHI) of the years 1991 and 2021 is delineated by the map. SUHI serves as a metric to gauge the disparity in temperature between urban areas and the surrounding rural regions. In fig. 11, the legend located at the lower section of

the illustration elucidates that measurements of SUHI are expressed in degrees Celsius (°C). In 1991 and 2021, the range of SUHI spanned from -3.0°C (cooler than the surrounding areas) to 3.0°C (warmer than the surrounding areas). Throughout the year 1991, the majority of the area exhibited values within the class -3.0 – 0.0 range, implying that the urban heat island effect results in slightly elevated temperatures in urban areas when compared to the adjacent rural areas.

However, there are certain regions on the map, particularly in the northern and western sections, that are depicted in darker shades of orange, indicating the opposite trend. In contrast to 1991, there appears to be a larger expanse falling within the range of class 1.5 – 3 to >3.0, signifying an intensification of the urban heat island effect. Furthermore, the areas colored in green are smaller in 2021 when compared to 1991.

The study area has undergone significant changes in land use and land cover over the past three decades, primarily due to economic progress and population growth. During the period from 1991 to 2021, the urban thermal feel variation index (UTFVI) in Bardez taluka exhibited a noticeable upward trend, indicating an increase in temperature fluctuations within urban areas. This increase has negative implications for the comfort of the residents, as the area of land that provides 'excellent' comfort, has decreased from 37.30 square kilometers (14.76%) in 1991 to 27.05 square kilometers (10.71%) in 2021, indicating a reduction of 4.05%.

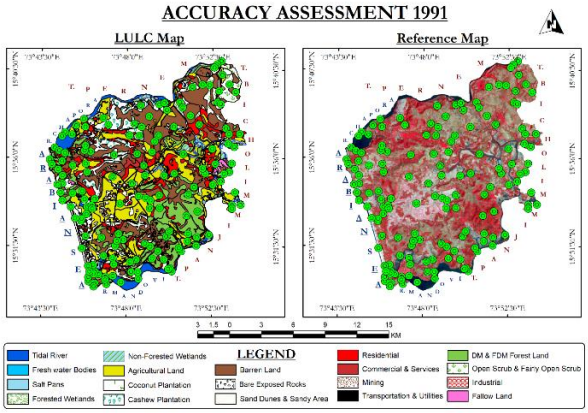

Figure 8: Accuracy Assessment 1991

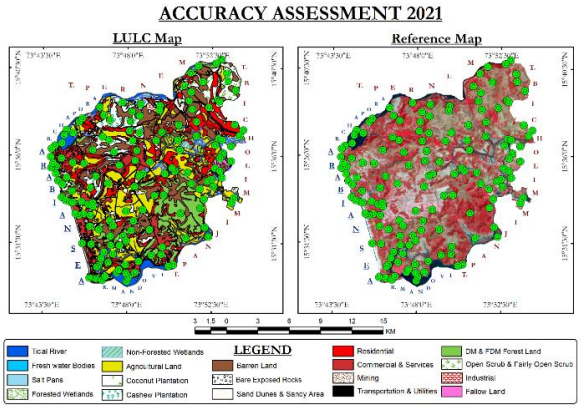

Figure 9: Accuracy Assessment 2021

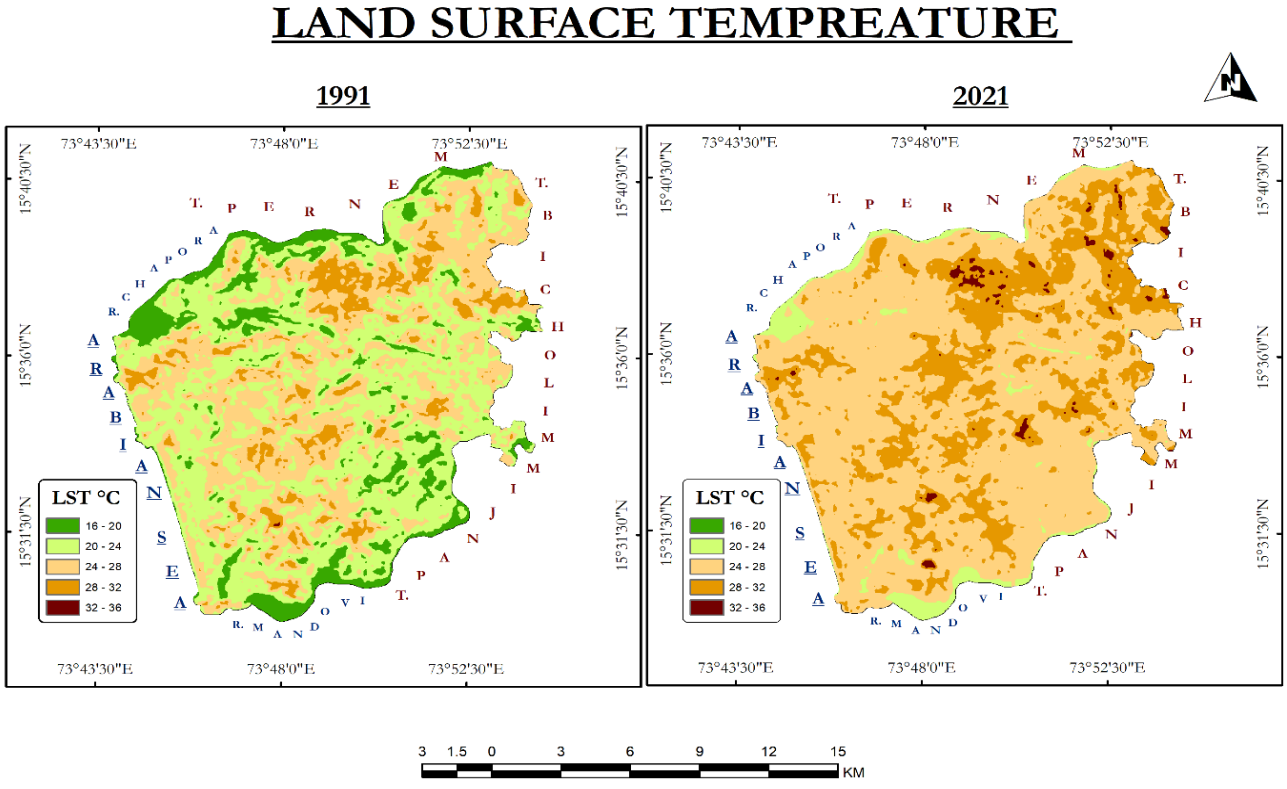

Figure 10: LST for the years 1991 and 2021

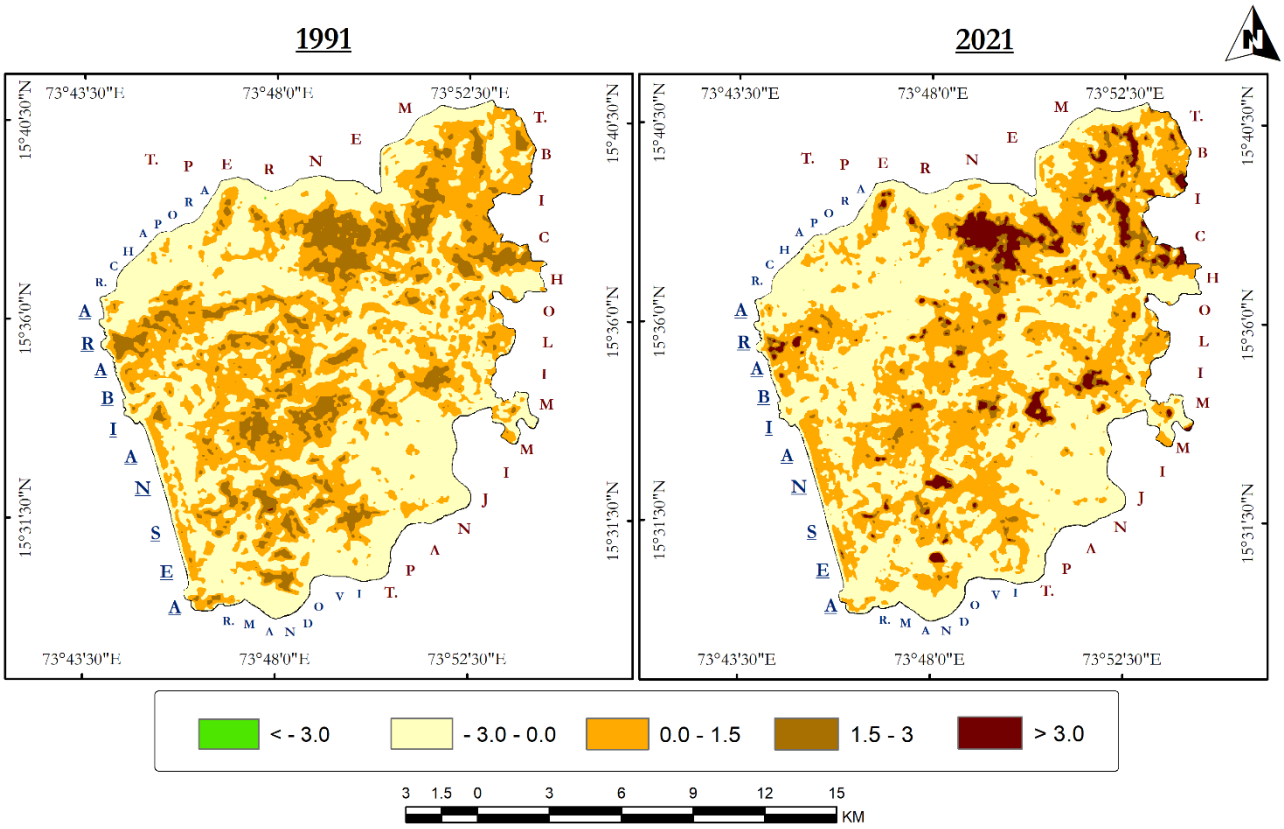

Figure 11: SUHI of the years 1991 and 2021

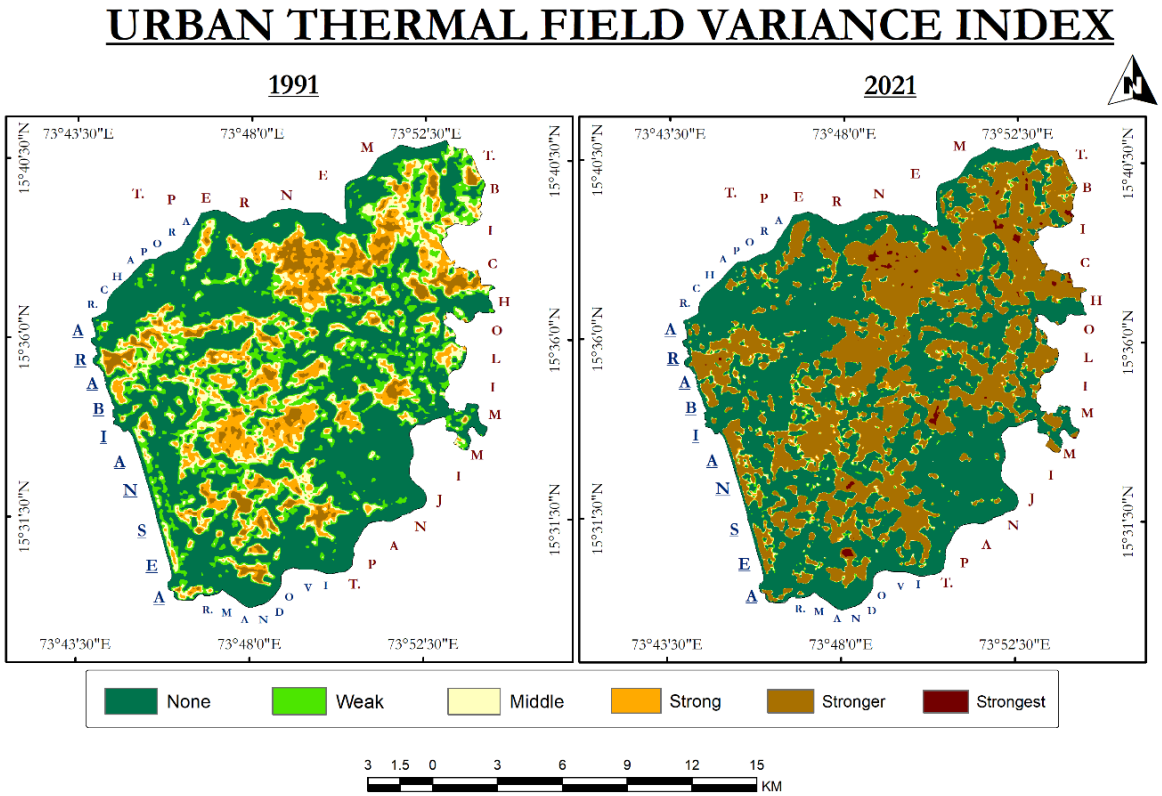

Figure 12: UTFVI of the year 1991 and 2021

On the other hand, the area with the lowest level of comfort has experienced an expansion from 13.98 square kilometers (5.54%) to 38.17 square kilometers (15.11%), representing a 9.57% increase during the same period (Table 4). These modifications are likely to be influenced by factors such as urbanization, impermeable surfaces like asphalt and concrete, towering structures and congested infrastructure, limited green spaces, altered microclimate, human activities such as industrial processes, transportation and energy consumption, which have the potential to generate urban heat islands and raise overall temperatures in cities, thereby impacting the comfort levels of the residents.

The surface urban heat island (SUHI) effect and worsening climatic conditions in urban areas are caused by increased LST. The urban thermal field variance index (UTFVI) phenomena provides a quantitative and qualitative description of the SUHI effect. A Pearson's correlation matrix is an adequate metric to establish a relationship between multiple variables.

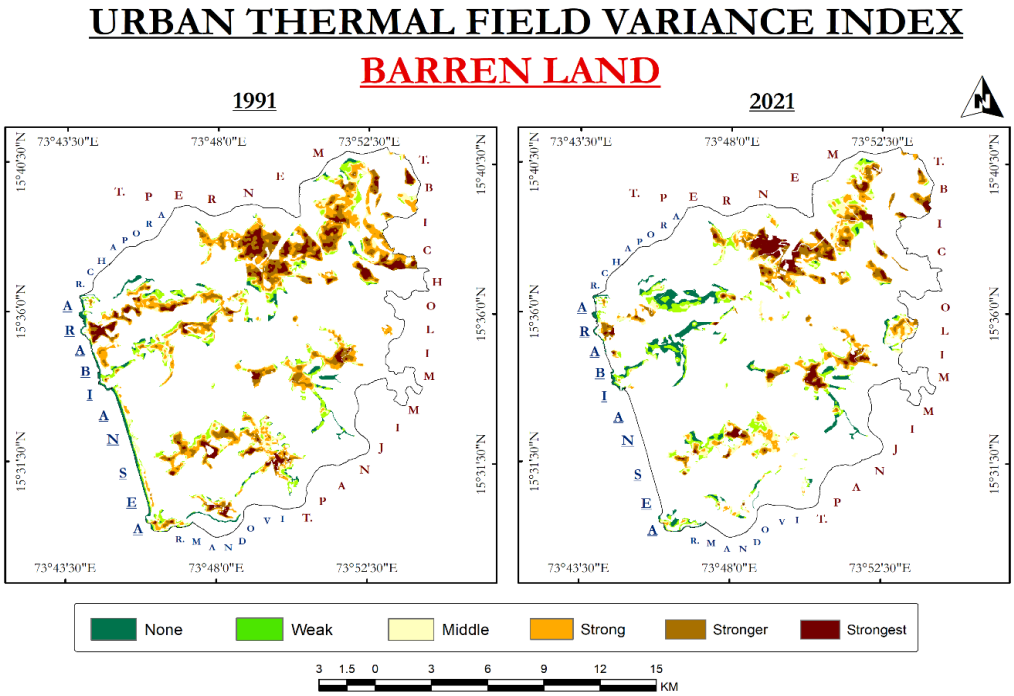

Figure 13: UTFVI of the year 1991 and 2021 Barren Land

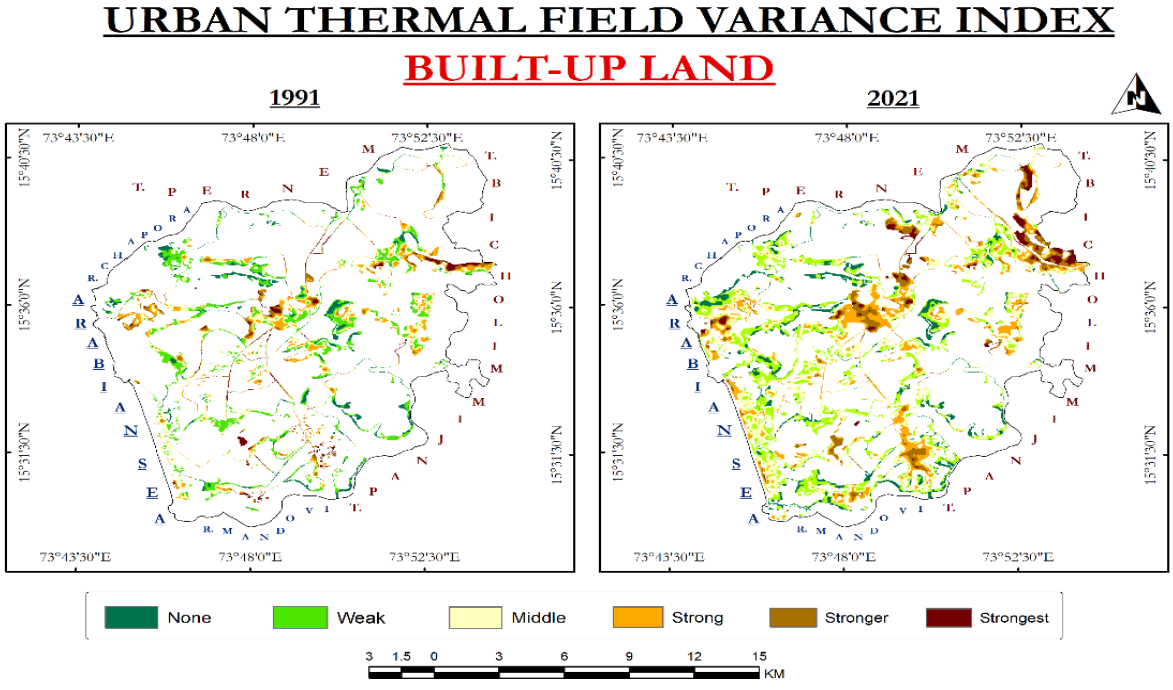

Figure 14: UTFVI of the year 1991 and 2021 Built-up Land

Table 4
Showing Urban Thermal Comfort Level for the year 1991 to 2021

Class	UTFVI	UTFVI Presence	Area Sq. Km. 1991	Area % 1991	Area Sq._Km. 2021	Area % 2021	UTCL
1	< 0	None	37.30	14.76	27.05	10.71	Excellent
2	0 – 0.005	Weak	59.84	23.68	50.89	20.14	Good
3	0.005 – 0.01	Middle	60.82	24.07	63.45	25.11	Normal
4	0.01 – 0.015	Strong	52.45	20.76	28.54	11.30	Bad
5	0.015 – 0.02	Stronger	28.27	11.19	44.56	17.64	Worse
6	> 0.2	Strongest	13.98	5.54	38.17	15.11	Worst
Total			**252.66**	**100**	**252.66**	**100**	

Matrix 3
Correlation Matrix 1991

Layer	LST	SUHI	UTFVI
LST	1.00000	0.97295	0.97295
SUHI	0.97295	1.00000	1.00000
UTFVI	0.97295	1.00000	1.00000

Matrix 4
Correlation Matrix 2021

Layer	LST	SUHI	UTFVI
LST	1.00000	0.94652	0.94652
SUHI	0.94652	1.00000	1.00000
UTFVI	0.94652	1.00000	1.00000

The diagonal elements are one because of the self-correlation and we can observe a strong correlation between LST, SUHI and UTFVI. The matrix refers to the conclusion that all the regions with higher LST experience higher SUHI and UTFVI. Also, the SUHI and UTVFI show a one-to-one correlation for both instances in 1991 and 2021.

t-test and f-test: Two separate groups were established for the analysis of land surface temperature (LST) in the study region for the years 1991 to 2021, as well as for the urban temperature field vertex index (UTFVI) in those same years. The average and variability of the groups were assessed using the t-test and f-test.

Parameters of t-test, f-test: The tests were performed at a 95% confidence level or 5% significance level.

Null Hypothesis for t-test: Two groups are independent random samples drawn from a normal distribution having equal means with unknown variance.

Null Hypothesis for f-test: Two groups are independent random samples drawn from a normal distribution having the same variance.

h=0: Null hypothesis cannot be rejected at the 5% significance level.
h=1: Null hypothesis can be rejected at a given confidence level i.e. there is no statistical evidence that the null hypothesis shall be accepted.

p: p, or probability expresses the likelihood that any observed variation across groups results from chance. The value ranges between 0-1.
ci for t-test: Confidence interval of the population mean with lower and upper bounds within a 95% confidence interval.
ci for f-test: Confidence interval of the ratios of variances with lower and upper bounds within a 95% confidence interval.
Statistic: The test statistic value.

The results show that the mean and the variance of LST for 1991 and 2021 of the entire study region are statistically significantly different at a 95% confidence level. In contrast, the UTFVI has the same mean for 1991 and 2021, but the variance is statistically significantly different.

Z-test: The z-test can be performed when the population standard deviation is known and the sample size is very large. Two LULC classes were segregated, namely, barren and the built-up. These classes were considered the sample and the entire region was considered a population for this sampled data. With the information on the LST and UTFVI standard deviation, two classes were compared with the population mean.

Parameters of z-test - Null Hypothesis for z-test: The sample is drawn from a normal distribution with the same mean and standard deviation as the populations.

h=0: Null hypothesis cannot be rejected at the 5% significance level.
h=1: Null hypothesis can be rejected at a given confidence level i.e. there is no statistical evidence that the null hypothesis shall be accepted.
p: p, or probability expresses the likelihood that any observed variation across groups results from chance. The value ranges between 0-1.
ci: Confidence interval of the population mean with lower and upper bounds within a 95% confidence interval.
Statistic: The test statistic value.

The results of z-tests performed on the samples specified in table 7 and table 8 suggest that the population mean and the sample mean are statistically significantly different for all the categories. The mean LST of barren and built-up areas is larger than the mean LST of the entire region. These LULC categories suffer from higher LST and higher UTFVI compared to the whole study area.

Conclusion

The study utilizes land surface temperature (LST) data and the urban thermal field variance index (UTFVI) to assess urban thermal comfort levels which are found to be adversely affected by increased temperature fluctuations in urban areas. The research highlights the impact of land use and land cover changes such as urbanization, impenetrable surfaces and reduced green areas, on the prevalence of urban heat islands and their negative effects on residents' comfort levels. The results of the analysis reveal significant shifts in land cover classes over the three decades with notable changes in areas such as coconut plantations, barren land, residential areas and commercial and services zones.

Table 5
Showing T-test of LST and UTFVI.

Categories	h	p	ci		Statistic t
LST	1	0	-8.0294	-7.9983	-1010.1
UTFVI	0	0.99998	-0.00025925	-0.00025925	-2.7975e-05

Table 6
Showing F-test of LST and UTFVI.

Categories	h	p	ci		Statistic t
LST	1	0	2.3875	2.4231	2.4052
UTFVI	1	0	0.018152	0.018423	0.018287

Table 7
Showing hypothesis testing for the years 1991 and 2021 of Barren Land and Built-up Land (LST).

Year	LULC Category	Population mean	Population Sigma	Sample mean	Sample Sigma	h	p	ci		z-Statistic
1991	Barren Land	21.345	3.5353	24.445	2.7925	1	0	24.418	24.472	226.12
	Built-up Land			21.266	2.4655	1	8.09e-06	21.232	21.301	-4.4626
2021	Barren Land	21.245	3.5353	30.759	2.6446	1	0	30.739	30.778	137.95
	Built-up Land			30.03	2.6446	1	0	30.014	30.046	82.081

Table 8
Showing hypothesis testing for the years 1991 and 2021 of Barren Land and Built-up Land (UTFVI).

Year	LULC Category	Population mean	Population Sigma	Sample mean	Sample Sigma	h	p	ci		z-Statistic
1991	Barren Land	-2.0355e-08	0.0093969	0.069488	0.007545	1	0	0.0083836	0.008525	234.28
	Built-up Land			-0.0003848	0.0066764	1	1.4e-16	-0.00047608	-0.00029351	-8.2615
2021	Barren Land	-1.6655e-08	0.069488	0.049753	0.07449	1	0	0.049147	0.050359	160.81
	Built-up Land			0.018627	0.07449	1	0	0.018138	0.019116	74.665

The findings suggest that these changes are largely driven by factors such as tourism-related activities, rapid urban expansion and infrastructure development. The urban heat islands in the Bardez Taluka region have led to significant alterations in land use and land cover, exacerbating urban thermal comfort issues. The study finds that the urban thermal feel variation index (UTFVI) has risen steadily throughout the analyzed time frame, reflecting increased temperature variations in urban areas. As a consequence, the proportion of land providing excellent thermal comfort has shrunk from 14.76% in 1991 to 10.71% in 2021 while areas with poorer comfort levels have expanded correspondingly. These trends are attributed to factors such as urbanization, impervious surfaces and insufficient greenery along with influences like tourism, infrastructure development and climate change.

To address these issues, it is suggested to carry out strategies that concentrate on intelligent urban planning, integrating porous surfaces, enhancing vegetation quality, reducing heat-generating activities, designing compact urban layouts and strategically placing buildings to improve natural ventilation and to minimize urban heat island impacts. Encouraging energy efficiency, responsible energy consumption and preserving green areas to mitigate urban heat island make impact on comfort levels.

References

1. Abebe G., Getachew D. and Ewunetu A., Analysing land use/land cover changes and its dynamics using remote sensing and GIS in Gubalafito district, Northeastern Ethiopia, *SN Appl. Sci.*, **4**, 1-15 **(2022)**

2. Abdul Athick A.S.M., Shankar K. and Naqvi H.R., Data on time series analysis of land surface temperature variation in response to vegetation indices in twelve Wereda of Ethiopia using mono window, split window algorithm and spectral radiance model, *Data Br.*, **27**, 104773 **(2019)**

3. Agapiou A., Estimating proportion of vegetation cover at the vicinity of archaeological sites using sentinel-1 and-2 data, supplemented by crowdsourced openstreetmap geodata, *Appl. Sci.* **10**, 1-17 **(2020)**

4. Agaton M., Setiawan Y. and Effendi H., Land Use/Land Cover Change Detection in an Urban Watershed: A Case Study of Upper Citarum Watershed, West Java Province, Indonesia, *Procedia Environ. Sci.*, **33**, 654–660 **(2016)**

5. Ahmed B., Kamruzzaman M.D., Zhu X., Shahinoor Rahman M.D. and Choi K., Simulating land cover changes and their impacts on land surface temperature in dhaka, Bangladesh, *Remote Sens.*, **5**, 5969–5998 **(2013)**

6. Al-Bayati A.H.I. and Jabbar S.A., The Use of Geospatial Technologies to Monitor the Variation of LULC for the Period from 1990 to 2020 for Some Agricultural Districts of Ramadi in Anbar Governorate – Iraq, IOP Conf. Ser. Earth Environ. Sci., 904 **(2021)**

7. Alshari E.A. and Gawali B.W., Development of classification system for LULC using remote sensing and GIS, *Glob. Transitions Proc.*, **2**, 8–17 **(2021)**

8. Anderson J.R., A Land Use And Land Cover Classification System For Use With Remote Sensor Data, United States Gov. Print. Off. **(1976)**

9. Ara S., Alif M.A.U.J. and Islam K.M.A., Impact of Tourism on LULC and LST in a Coastal Island of Bangladesh: A Geospatial Approach on St. Martin's Island of Bay of Bengal, *J. Indian Soc. Remote Sens.*, **49**, 2329–2345 **(2021)**

10. Avdan U. and Jovanovska G., Algorithm for automated mapping of land surface temperature using LANDSAT 8 satellite data, *J. Sensors*, **2016**, 1-8 **(2016)**

11. Bisht B.S. and Kothyari B.P., Land-cover change analysis of Garur Ganga watershed using GIS/remote sensing technique, *J. Indian Soc. Remote Sens.*, **29**, 137–141 **(2001)**

12. Brown D.G., Pijanowski B.C. and Duh J.D., Modeling the relationships between land use and land cover on private lands in the Upper Midwest, USA, *J. Environ. Manage.*, **59**, 247–263 **(2000)**

13. Cevik Degerli B. and Cetin M., Evaluation of UTFVI index effect on climate change in terms of urbanization, *Environ. Sci. Pollut. Res.*, **30**, 75273–75280 **(2023)**

14. Chen H. et al, Changes of the spatial and temporal characteristics of land-use landscape patterns using multi-temporal Landsat satellite data: A case study of Zhoushan Island, China, *Ocean Coast. Manag.*, **213**, 105842 **(2021)**

15. Choudhury D., Das K. and Das A., Assessment of land use land cover changes and its impact on variations of land surface temperature in Asansol-Durgapur Development Region, *Egypt. J. Remote Sens. Sp. Sci.*, **22**, 203–218 **(2019)**

16. Congalton R.G., A review of assessing the accuracy of classifications of remotely sensed data, *Remote Sens. Environ.*, **37**, 35–46 **(1991)**

17. Ding H. and Shi W., Land-use/land-cover change and its influence on surface temperature: a case study in Beijing City, *Int. J. Remote Sens.*, **34**, 5503–5517 **(2013)**

18. Elhabodi T.S. et al, A review on BIPV-induced temperature effects on urban heat islands, *Urban Clim.*, **50**, 101592 **(2023)**

19. Elhag M., Consideration of Landsat-8 Spectral Band Combination in Typical Mediterranean Forest Classification in Halkidiki, Greece, *Open Geosci.*, **9**, 468–479 **(2017)**

20. Esha E.J. and Rahman M.T.U., Simulation of future land surface temperature under the scenario of climate change using remote sensing and GIS techniques of northwestern Rajshahi district, Bangladesh, *Environ. Challenges*, **5**, 100365 **(2021)**

21. Ewunetu A., Simane B., Teferi E. and Zaitchik B.F., Mapping and quantifying comprehensive land degradation status using spatial multicriteria evaluation technique in the headwaters area of upper blue nile river, *Sustain.*, **13**, 1–28 **(2021)**

22. Foody G.M., Explaining the unsuitability of the kappa coefficient in the assessment and comparison of the accuracy of thematic maps obtained by image classification, *Remote Sens. Environ.*, **239**, 111630 **(2020)**

23. Fu P. and Weng Q., A time series analysis of urbanization induced land use and land cover change and its impact on land surface temperature with Landsat imagery, *Remote Sens. Environ.*, **175**, 205–214 **(2016)**

24. Galve J.M. et al, Assessment of Land Surface Temperature Estimates from Landsat 8-TIRS in A High-Contrast Semiarid Agroecosystem. Algorithms Intercomparison, *Remote Sens.*, **14**, 1-22 **(2022)**

25. Gandhi G.M., Parthiban S., Thummalu N. and Christy A., Ndvi: Vegetation Change Detection Using Remote Sensing and Gis - A Case Study of Vellore District, *Procedia Comput. Sci.*, **57**, 1199–1210 **(2015)**

26. García D.H. and Díaz J.A., Space–time analysis of the earth's surface temperature, surface urban heat island and urban hotspot: relationships with variation of the thermal field in Andalusia (Spain), *Urban Ecosyst.*, **26**, 525–546 **(2023)**

27. Guida Johnson B. and Zuleta G.A., Land-use land-cover change and ecosystem loss in the Espinal ecoregion, Argentina, *Agric. Ecosyst. Environ.*, **181**, 31–40 **(2013)**

28. Guha S., Govil H., Dey A. and Gill N., Analytical study of land surface temperature with NDVI and NDBI using Landsat 8 OLI and TIRS data in Florence and Naples city, Italy, *Eur. J. Remote Sens.*, **51**, 667–678 **(2018)**

29. Gumma M.K., Thenkabail P.S., Teluguntla P. and Whitbread A.M., Indo-ganges river basin land use/land cover (LULC) and irrigated area mapping. Indus River Basin: Water Security and Sustainability, Elsevier Inc., doi:10.1016/B978-0-12-812782-7.00010-2 **(2019)**

30. Hamad R., An Assessment of Artificial Neural Networks, Support Vector Machines and Decision Trees for Land Cover Classification Using Sentinel-2A Data, *Appl. Ecol. Environ. Sci.*, **8**, 459–464 **(2020)**

31. Hidalgo-García D. and Arco-Díaz J., Modeling the Surface Urban Heat Island (SUHI) to study of its relationship with variations in the thermal field and with the indices of land use in the metropolitan area of Granada (Spain), *Sustain. Cities Soc.*, **87**, 1-16 **(2022)**

32. Ibrahim G.R.F., Urban land use land cover changes and their effect on land surface temperature: Case study using Dohuk City in the Kurdistan Region of Iraq, *Climate*, **5**, 1-18 **(2017)**

33. Kafer P.S., Rolim S.B.A., Iglesias M.L., Da Rocha N.S. and Diaz L.R., Land surface temperature retrieval by landsat 8 thermal band: Applications of laboratory and field measurements, *IEEE J. Sel. Top. Appl. Earth Obs. Remote Sens.*, **12**, 2332–2341 **(2019)**

34. Kafy A. Al et al, Prediction of seasonal urban thermal field variance index using machine learning algorithms in Cumilla, Bangladesh, *Sustain. Cities Soc.*, **64**, 102542 **(2021)**

35. Khan M.S., Ullah S., Sun T., Rehman A.U. and Chen L., Land-use/land-cover changes and its contribution to urban heat Island: A case study of Islamabad, Pakistan, *Sustain.*, **12**, 1-17 **(2020)**

36. Khandelwal S., Goyal R., Kaul N. and Mathew A., Assessment of land surface temperature variation due to change in elevation of area surrounding Jaipur, 37 India, *Egypt. J. Remote Sens. Sp. Sci.*, **21**, 87–94 **(2018)**

37. Krishna T.H., Ramana R.V. and Jeyakanthan V.S., Accuracy assessment of land use and land cover by using GIS and RS, International conference on Recent Development in Engineering Scienes, Humanites and Management, **1**, 135–143 (2020)

38. Liu L. and Zhang Y., Urban heat island analysis using the Landsat TM data and ASTER Data: A case study in Hong Kong, *Remote Sens.*, **3**, 1535–1552 **(2011)**

39. Majumder A. et al, Estimation of land surface temperature using different retrieval methods for studying the spatiotemporal variations of surface urban heat and cold islands in Indian Punjab, *Environ. Dev. Sustain.*, **23**, 15921–15942 **(2021)**

40. Moisa M.B. and Gemeda D.O., Assessment of urban thermal field variance index and thermal comfort level of Addis Ababa metropolitan city, Ethiopia, *Heliyon*, **8**, e10185 **(2022)**

41. Mondal A., Guha S. and Kundu S., Dynamic status of land surface temperature and spectral indices in Imphal city, India from 1991 to 2021, *Geomatics, Nat. Hazards Risk*, **12**, 3265–3286 **(2021)**

42. Nadaf F.M. and Gaonkar V.G.P., Spatio-temporal monitoring and predicting the Land Use/Land Cover Transformations using Cellular Automata (CA)–Markov Model: A case study of Urban Canacona, Goa India, *Bull. Env. Pharmacol. Life Sci*, **10(10)**, 204-213 **(2021)**

43. Nagendra H. and Utkarsh G., Landscape ecological planning through a multi-scale characterization of pattern: Studies in the Western Ghats, South India, *Environ. Monit. Assess.*, **87**, 215–233 **(2003)**

44. Naim M.N.H. and Kafy A.A., Assessment of urban thermal field variance index and defining the relationship between land cover and surface temperature in Chattogram city: A remote sensing and statistical approach, *Environ. Challenges*, **4**, 100107 **(2021)**

45. Neinavaz E., Skidmore A.K. and Darvishzadeh R., Effects of prediction accuracy of the proportion of vegetation cover on land surface emissivity and temperature using the NDVI threshold method, *Int. J. Appl. Earth Obs. Geoinf.*, **85**, 101984 **(2020)**

46. Ojeh V.N., Yusuf M.B. and Bako S.L., Impact of Urbanization on Land use and Land Cover Changes in Growing Cities of Rwanda, *J. Korean Soc. Environ. Eng.*, **44**, 258–266 **(2022)**

47. Prabhu Gaonkar V.G. et al, Analysing Spatio-temporal Changes in Land Surface Temperature of Coastal Goa Using LANDSAT Satellite Data, Ecological Footprints of Climate Change, Springer, Cham, doi:10.1007/978-3-031-15501-7_20, 517–541 **(2022)**

48. Qin Z., Karnieli A. and Berliner P., A mono-window algorithm for retrieving land surface temperature from Landsat TM data and

its application to the Israel-Egypt border region, *Int. J. Remote Sens.*, **22**, 3719–3746 **(2001)**

49. Qu S. et al, Distinguishing the impacts of climate change and anthropogenic factors on vegetation dynamics in the Yangtze River Basin, China, *Ecol. Indic.*, **108**, 105724 **(2020)**

50. Renard F., Alonso L., Fitts Y., Hadjiosif A. and Comby J., Evaluation of the effect of urban redevelopment on surface urban heat islands, *Remote Sens.*, **11**, 1-37 **(2019)**

51. Rosado R.M.G. et al, Mapping the LST (Land Surface Temperature) with Satellite Information and Software ArcGis, IOP Conf. Ser. Mater. Sci. Eng., 811 **(2020)**

52. Rozario P.F., Oduor P., Kotchman L. and Kangas M., Transition Modeling of Land-Use Dynamics in the Pipestem Creek, North Dakota, USA, *J. Geosci. Environ. Prot.*, **5**, 182–201 **(2017)**

53. Rosenfield G.H. and Fitzpatrick-Lins K., A coefficient of agreement as a measure of thematic classification accuracy, *Photogramm. Eng. Remote Sens.*, **52**, 223–227 **(1986)**

54. Rwanga S.S. and Ndambuki J.M., Accuracy Assessment of Land Use/Land Cover Classification Using Remote Sensing and GIS, *Int. J. Geosci.*, **8**, 611–622 **(2017)**

55. Sahana M., Dutta S. and Sajjad H., Assessing land transformation and its relation with land surface temperature in Mumbai city, India using geospatial techniques, *Int. J. Urban Sci.*, **23**, 205–225 **(2019)**

56. Scolozzi R. and Geneletti D., A multi-scale qualitative approach to assess the impact of urbanization on natural habitats and their connectivity, *Environ. Impact Assess. Rev.*, **36**, 9–22 **(2012)**

57. Schmidt J.J., Piras E. and Weller G., Environmental social science: human–environment interactions and sustainability, *Int. J. Soc. Res. Methodol.*, **15**, 445–450 **(2012)**

58. Sekertekin A. and Bonafoni S., Land surface temperature retrieval from Landsat 5, 7 and 8 over rural areas: Assessment of different retrieval algorithms and emissivity models and toolbox implementation, *Remote Sens.*, **12**, 1-32 **(2020)**

59. Sliuzas R., Kuffer M. and Masser I., The spatial and temporal nature of urban objects, *Remote Sens. Digit. Image Process.*, **10**, 67–84 **(2010)**

60. Sobrino J.A. and Irakulis I., A methodology for comparing the surface urban heat Island in selected urban agglomerations around the world from Sentinel-3 SLSTR data, *Remote Sens.*, **12**, 1-29 **(2020)**

61. Song J. et al, Effects of building density on land surface temperature in China: Spatial patterns and determinants, *Landsc. Urban Plan.*, **198**, 103794 **(2020)**

62. Sundell D. and Rämä M., A methodology for systematic mapping of heat sources in an urban area, *Clean Technol. Environ. Policy*, **24**, 2991–3001 **(2022)**

63. Tan K., Liao Z., Du P. and Wu L., Land surface temperature retrieval from Landsat 8 data and validation with geosensor network, *Front. Earth Sci.*, **11**, 20–34 **(2017)**

64. Taloor A.K., Drinder Singh Manhas and Chandra Kothyari G., Retrieval of land surface temperature, normalized difference moisture index, normalized difference water index of the Ravi basin using Landsat data, *Appl. Comput. Geosci.*, **9**, 100051 **(2021)**

65. Tamouk J., Lotfi N. and Farmanbar M., Satellite image classification methods and Landsat 5TM bands, *arXiv*, https://doi.org/10.48550/arXiv.1308.1801 **(2013)**

66. Tayfun Kindap et al, Quantification of the Urban Heat Island Under a Changing Climate over Anatolian Peninsula, *Intech*, **i**, 13 **(2012)**

67. Ullah W. et al, Analysis of the relationship among land surface temperature (LST), land use land cover (LULC) and normalized difference vegetation index (NDVI) with topographic elements in the lower Himalayan region, *Heliyon*, **9**, e13322 **(2023)**

68. Vibhute A., Vibhute A.D. and Gawali B.W., Analysis and modeling of agricultural land use using remote sensing and geographic information system: a review, *Int. J. Eng. Res. Appl.*, **3**, 81–91 **(2013)**

69. Wang H., Zhang Y., Tsou J.Y. and Li Y., Surface urban heat island analysis of shanghai (China) based on the change of land use and land cover, *Sustain*, **9**, 1-22 **(2017)**

70. Weng Q., Lu D. and Schubring J., Estimation of land surface temperature-vegetation abundance relationship for urban heat island studies, *Remote Sens. Environ.*, **89**, 467–483 **(2004)**

71. Wemegah C.S., Yamba E.I., Aryee J.N.A., Sam F. and Amekudzi L.K., Assessment of urban heat island warming in the greater accra region, *Sci. African*, **8**, e00426 **(2020)**

72. Yue W., Xu J., Tan W. and Xu L., The relationship between land surface temperature and NDVI with remote sensing: Application to Shanghai Landsat 7 ETM+ data, *Int. J. Remote Sens.*, **28**, 3205–3226 **(2007)**

73. Yuvaraj R.M., Extents of Predictors for Land Surface Temperature Using Multiple Regression Model, *Sci. World J.*, **2020**, 1-10 **(2020)**

74. Yu Z.D.L. et al, Selection of landsat 8 OLI band combinations for land use and land cover classification, 2019 8th Int. Conf. Agro-Geoinformatics, Agro-Geoinformatics **(2019)**

75. Zhang Y. and Sun L., Spatial-temporal impacts of urban land use land cover on land surface temperature: Case studies of two Canadian urban areas, *Int. J. Appl. Earth Obs. Geoinf.*, **75**, 171–181 **(2019)**

76. Zhao W. et al, An analysis of land surface temperature trends in the Central Himalayan region based on MODIS products, *Remote Sens.*, **11**, 1-19 **(2019)**.

(Received 06th October 2024, accepted 04th December 2024)